Journal of Power Sources 185 (2008) 815–821

Contents lists available at ScienceDirect

Journal of Power Sources

journal homepage: www.elsevier.com/locate/jpowsour

High nitrogen stainless steel as bipolar plates for proton exchange membrane fuel cells

Masanobu Kumagai [a], Seung-Taek Myung [b], Ryo Asaishi [b], Yasuyuki Katada [c], Hitoshi Yashiro [b,*]

[a] Taiyo Stainless Spring Co., Ltd., 2-8-6 Shakujiicho, Nerimaku, Tokyo 177-0041, Japan
[b] Department of Chemical Engineering, Iwate University, 4-3-5 Ueda, Morioka, Iwate 020-8551, Japan
[c] National Institute for Materials Science, 1-2-1 Sengen, Tsukuba, Ibaraki 305-0047, Japan

ARTICLE INFO

Article history:
Received 5 June 2008
Accepted 11 July 2008
Available online 26 July 2008

Keywords:
High nitrogen stainless steel
Bipolar plate
Fuel cell
Corrosion
XPS

ABSTRACT

To investigate the applicability of high nitrogen (HN) austenitic stainless steel as bipolar plates for proton exchange membrane fuel cells (PEFCs), the polarization tests were carried out in synthetic solutions (0.05 M SO_4^{2-} (pHs 2.3, 4.3 and 5.5) +2 ppm F^-) at 353 K. Interfacial contact resistance between the stainless steel and gas diffusion layer was measured before and after polarization. A single cell employing the HN stainless steel as bipolar plates was operated for 1000 h at 0.5 A cm^{-2} (12.5 A). The single cell exhibited voltage drop of 17 mV during the operation. Corrosion products were scarcely detected for the HN stainless steel bipolar plate, as confirmed by scanning electron microscopy. After the polarization tests and single cell operation, XPS analyses were carried out to examine the resulting surface states. In the synthetic solutions to pH 4.3, the passive films mainly consisted of oxides enriched with Cr. When the solution pH was 5.5, on the other hand, the films were mainly composed of Fe-oxides. After the single cell operation for 1000 h, it was found that the passive films of the rib surface for the gas inlet part was mainly composed by Fe-oxides. On the other hand, the passive films for the ribs from center to gas outlet part were mainly made up of Cr-oxides. By combining the simulated and real operation environments, it is believed that the corrosion resistive Cr-oxides passive layer of the HN stainless steel obtained by the presence of nitrogen incorporated into the stainless steel could contribute to the maintenance of the higher cell voltage during the extensive cell operation.

1. Introduction

Proton exchange membrane fuel cells (PEFCs) are systems that use hydrogen and oxygen or air and they transform chemical energy into electrical energy [1]. The PEFCs consist of membrane electrode assembly (MEA) and bipolar plates. The bipolar plate is a multifunctional component of PEFCs. Ideal material for bipolar plates should have high corrosion resistance, high electrical conductivity, chemical stability and heat stability.

Several groups proposed the applicability of stainless steels for bipolar plates [2–7]. It is generally believed that austenitic stainless steels have high corrosion resistance in the PEFC environments compared with ferritic and martensitic stainless steels. However, stainless steels are usually faced on general corrosion and/or crevice corrosion where SO_4^{2-} and F^- ions are released from the membrane in the PEFCs. Additions of nickel, chromium, and molybdenum are effective ways to improve corrosion resistance [8,9]. However, those are rare elements and relatively expensive.

Nitrogen is of interest as a substituent for nickel in stainless steel. Introduction of nitrogen into steel has a couple of advantages: (a) the nitrogen element is abundant in nature, which is contained around 80% in air; (b) the presence of nitrogen in stainless steels enhances mechanical properties and gives rise to the improvement of corrosion resistance. Inexpensive nitrogen, thus, is possible to substitute for expensive nickel ingredient. For examples, Strecher reported [10] that the nitrogen improved the localized corrosion resistance of austenitic stainless steel as a result of the stabilization of austenitic layers. Lu et al. explained [11] that nitrogen was concentrated to the metal side of interface between passive film and stainless steel. Pawel et al. [12] suggested that nitrogen not only facilitated dissolution of iron but concentrated chromium in the passive film. According to previous reports, nitrogen in stainless steel after the polarization in chloride solution dissolves as NO_3^- [13] or NH_4^+ [8,14,15]. Osozawa reported that the existence of NO_3^- can be traced if the polarization is carried out up to noble potential [16]. Wang and Turner [17] introduced that nitrogen-bearing

* Corresponding author. Tel.: +81 19 621 6330; fax: +81 19 621 6330.
E-mail address: yashiro@iwate-u.ac.jp (H. Yashiro).

0378-7753/$ – see front matter © 2008 Elsevier B.V. All rights reserved.
doi:10.1016/j.jpowsour.2008.07.041

Table 1
Chemical composition of the HN stainless steel (mass%)

	HN
C	0.022
Si	0.0005
Mn	3.09
Cr	24.07
Ni	3.88
Mo	1.94
N	1.06
Fe	Bal.

stainless steels (AISI Type 201 and AL219) are promising materials for PEFC bipolar plates, although the nitrogen content in the steels were around 0.3%.

Recently, high nitrogen stainless steel (hereafter referred to HN stainless steel) has been developed in NIMS, Japan [18]. Fairly high amount of nitrogen (~1 mass% shown in Table 1) was incorporated into the austenitic metal bulk that shows no precipitation of nitride in the matrix of stainless steel. In this study, the HN stainless steel was investigated to apply for PEFCs. Here, we would like to report the applicability of the HN stainless steel as bipolar plates for PEFCs.

2. Experimental

The HN stainless steel was obtained by using pressurized electro-slag remelting system [18]. The chemical composition of the HN stainless steel is described in Table 1. Besides 24 mass% of chromium, relatively small amount of nickel and manganese was added to ensure the complete solution of high level of nitrogen. About 2% molybdenum was also employed expecting the synergetic effect with nitrogen against corrosion. The HN stainless steel plates were machined into a square (20 mm × 20 mm × 2 mm) and mounted into epoxy resin for the polarization tests. The surfaces were finished using diamond paste polisher of 6 μm and cleaned ultrasonically in hexane for 15 min.

Polarization tests were carried out in PTFE lined cells, which were filled with 200 cm^3 of 0.05 M SO_4^{2-} (pHs 2.3, 4.3 and 5.5) +2 ppm F^- solution saturated with either Ar (dynamic mode: −500 mV to 1500 mV with a sweep rate of 60 mV min^{-1}) or air (transient mode: at +600 mV for 8 h) to simulate the PEFC environments [2]. A reference electrode (SCE) was placed out of the water bath, which kept the temperature of the cell to 353 K. Prior to the polarization test, specimens were first cathodically treated at −500 mV (SCE) to remove air-formed oxide films.

The HN stainless steel (80 mm × 80 mm × 6 mm) was machined into a bipolar plate with serpentine flow field according to the NEDO report by JARI [19]. The surfaces of bipolar plates were also finished using diamond paste polisher of 6 μm and cleaned ultrasonically in hexane for 15 min. The active electrode area was 50 mm × 50 mm. A single cell was assembled using the as-polished HN stainless steel bipolar plates and a commercially available membrane electrode assembly that adopts carbon cloth as a gas diffusion layer (GDL) with compressive force of 200 N cm^{-2} controlled by a torque wrench. The as-built single cell was operated at 348 K under ambient pressure. The reactant gases were fully humidified at 343 K. The utilization was 70% for the fuel gas (H_2) and 40% for air. The applied current density was 0.5 A cm^{-2} (12.5 A).

After the polarization tests and cell operations, the surfaces of the HN stainless steel were analyzed by X-ray photoelectron spectroscopy (XPS, ULVAC-PHI 5600) with a monochromatic Al Kα source. The take-off angle of the emitted photoelectrons was adjusted usually to 45° with respect to the surface. The depth scale for sputtering was calibrated relative to anodically formed SiO_2 standard layers. The sputter rate was determined to be 2.7 nm min^{-1} for the applied conditions of the Ar-ion gun. Binding energies of XPS-peaks of standards referred to the literature [20].

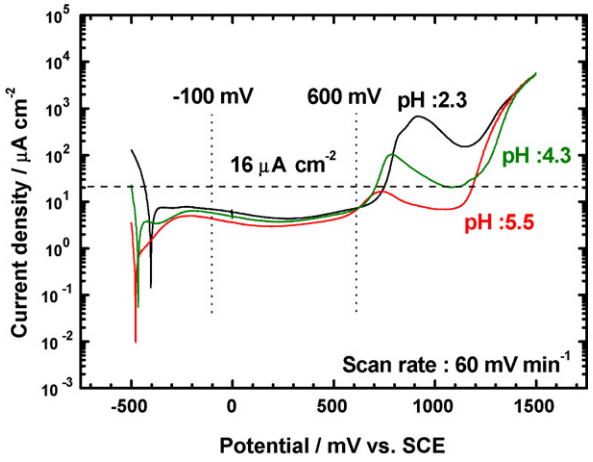

Fig. 1. Anodic polarization curves for the HN stainless steel in deaerated 0.05 M SO_4^{2-} (pHs 2.3, 4.3 and 5.5) +2 ppm F^- solutions at 353 K.

3. Results and discussion

Fig. 1 shows anodic polarization curves for the HN stainless steel in a deaerated 0.05 M SO_4^{2-} (pHs 2.3, 4.3 and 5.5) +2 ppm F^- solution at 353 K (simulated PEFC environment). Corrosion potential was shifted to less noble direction and the passive current density decreased with increasing the solution pH. Similar phenomena appeared for the type 310S stainless steel [21]. The HN stainless steel satisfies the required corrosion rate of <16 μA cm^{-2} in Fig. 1 [22]. The low passive current density in passive region indicates good corrosion resistance.

Since general corrosion is readily observed in the cathode side [21], the transient polarization tests were performed in the synthesized cathodic condition. Fig. 2 shows the current density versus time curves for the HN stainless steel polarized at 600 mV (SCE) in synthetic solutions with different pHs (pHs 2.3, 4.3 and 5.5), where the potential of 600 mV is considered as a typical cathodic potential under the PEFC environment [2]. Generally, corrosion resistance is closely related with its passive current density during the polarization. The current density of the HN stainless steel at +600 mV (SCE) rapidly decreased during the transient polarization in Fig. 2. The

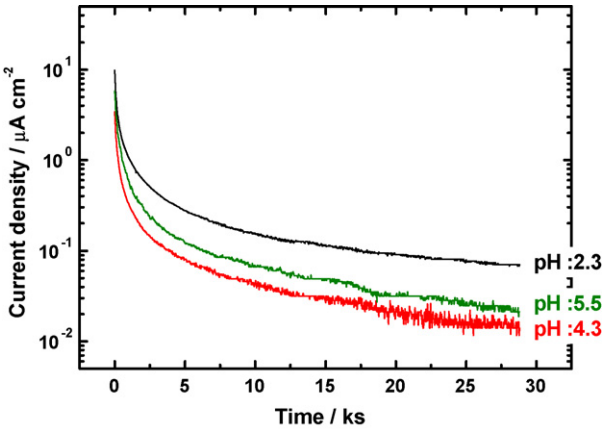

Fig. 2. Effect of pH on time variation of anodic current density at +600 mV for the HN stainless steel in aerated 0.05 M SO_4^{2-} +2 ppm F^- solutions at 353 K.

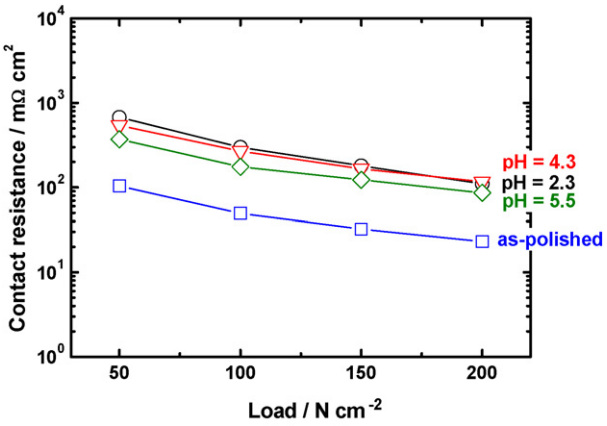

Fig. 3. Contact resistance between the HN stainless steel and carbon cloth after polarization at +600 mV for 8 h in 0.05 M SO_4^{2-} (pHs 2.3, 4.3 and 5.5) +2 ppm F^- solutions at 353 K.

passive current density was lower at higher pHs. The observed current density at pH 5.5 is slightly higher than that of pH 4.3, due to earlier onset of the transpassive dissolution at pH 5.5 as indicated in Fig. 1. No remarkable change in the current was seen during the polarization tests for 8 h irrespective of pH values, implying that crucial corrosion did not occur.

Fig. 3 shows the interfacial contact resistance (ICR) between the HN stainless steel and carbon cloth GDL before and after the polarization at 600 mV (SCE) for 8 h. The measurement method was referred from the literature [3]. The measured ICR values of the HN stainless steels decreased with increasing applied force. The polarized steels exhibited slightly higher ICR values, compared with those of the as-polished. This implies that the resulting passive films of the HN stainless steel have different surface structure from the as-polished state after the polarization. No significant changes were seen in the ICR values when the polarizations were done at pHs 2.3 and 4.3. A little lower ICR values were obtained at pH 5.5. Such changes in ICR can be related to the thickness and chemical composition of the resulting passive layers.

The structure of passive layer on stainless steel varies depending on the surrounding environment. Therefore, surface analysis of passive films would enable one to infer the environment under which the stainless steel had been exposed [23]. Fig. 4a and b show the XPS spectra for Fe2p and Cr2p orbitals of the polarized HN stainless steel in the simulated conditions, respectively. For N1s, we could not successfully distinguish the matrix-originated peak (around 396 eV) from the contamination around 400 eV. Ar-ion sputtering gave the elimination of the contamination, resulting in the presence of nitrogen in the metal (Fig. 6a–d). For the Fe2p spectra (Fig. 4a), the as-polished HN stainless steel showed a peak around 707 eV, which corresponds to Fe metal ascribed to the metal bulk. Fe-oxides such as FeO, Fe_3O_4, Fe_2O_3, which compose the air-formed passive layer, were also observed at around 711 eV. Similarly to the Fe ingredient, the as-polished HN stainless steel exhibited Cr metal-related peak at around 574 eV, and a trivalent Cr-oxide peak was also seen at around 577 eV in Fig. 4b. The cationic ratio of Cr-oxide versus Fe-oxides determined from the XPS spectra before sputtering was 0.36 (Fig. 5). Depth profile for the as-polished steel (Fig. 6a) indicates that the surface of the HN stainless steel is mainly covered with oxide layers such compounds as Cr and Fe oxides. The air-formed oxide layers almost disappeared after sputtering about 50 s, indicating that the resulting thickness of the air-formed oxide layer would be approximately 2.5 nm.

The Fe metal-related peak appeared for the polarized steel at pHs 2.3 and 4.3 in Fig. 4a, and Cr-oxide was strongly observed at

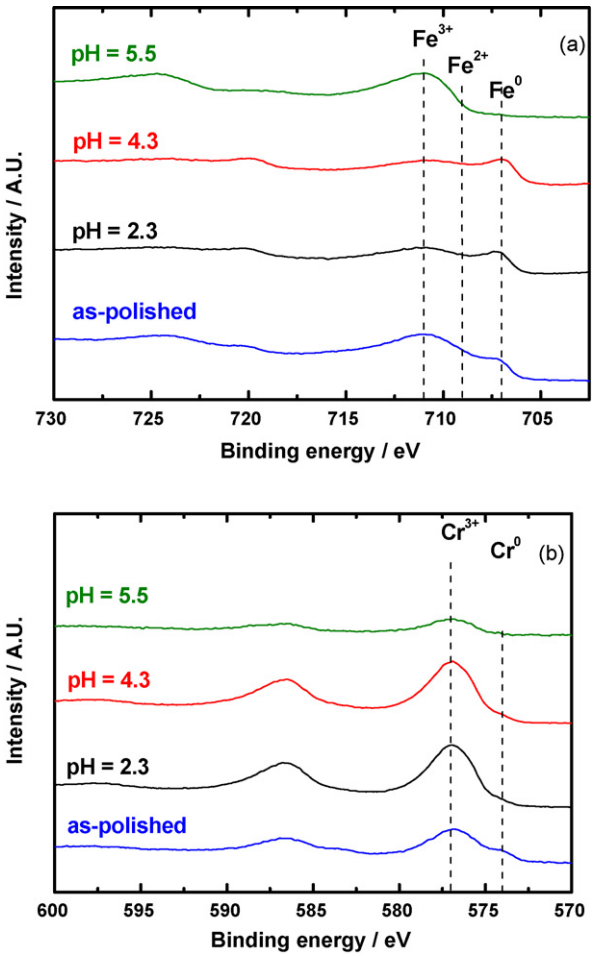

Fig. 4. XPS spectra of (a) Fe2p and (b) Cr2p for the HN stainless steel after 8 h polarization at +600 mV for 8 h in 0.05 M SO_4^{2-} (pHs 2.3, 4.3 and 5.5) +2 ppm F^- solutions at 353 K.

those pH values in Fig. 4b. This indicates that the Fe-oxides are soluble at those pH values so that Fe metal coming from the HN stainless steel bulk is observed, implying that the formed passive layer is thin. Moreover, the Cr-oxide component was highly concentrated on the outermost surface at pH 4.3 in Fig. 5. This says that the passive film is mainly composed of Cr-oxide in the pH range. The calculated

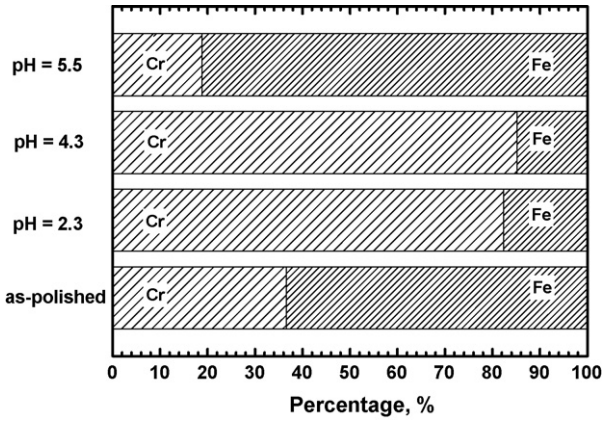

Fig. 5. Cr/Fe oxides cationic ratio from the outermost oxide layer based on XPS analysis for the HN stainless steel polarized at +600 mV for 8 h in 0.05 M SO_4^{2-} (pHs 2.3, 4.3 and 5.5) +2 ppm F^- solutions at 353 K.

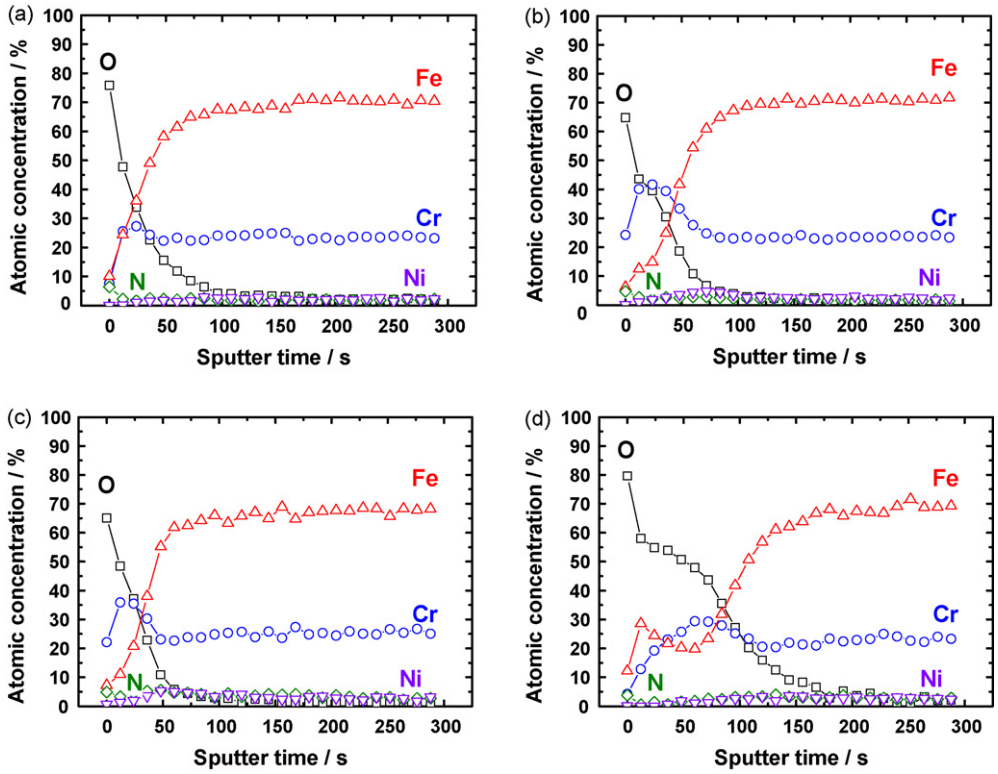

Fig. 6. XPS depth profiles of (a) as-polished the HN stainless steel and polarized steel at +600 mV for 8 h in 0.05 M SO_4^{2-} +2 ppm F^- solutions at 353 K: (b) pH 2.3, (c) pH 4.3 and (d) pH 5.5.

cationic ratio of Cr-oxide versus Fe-oxides was approximated to 0.8 at both pHs 2.3 and 4.3 in Fig. 5. In depth profile for the pH 2.3 (Fig. 6b), the atomic concentration of Cr ingredient was maximized by 42% by sputtering for 24 s, whereas the concentration of Fe ingredient was smaller of about 15% at the same condition. The thickness of the passive layer was found to be about 3.5–4.5 nm. At pH 4.3, the maximum atomic concentration of Cr somewhat decreased to 35%, but Fe concentration slightly increased by 20% by sputtering for 24 s in Fig. 6c. The eliminated thickness of the passive film was estimated as to be 4–5 nm. It is likely that the structure and chemical composition of the passive layer at pHs 2.3 and 4.3 seems to be quite similar to each other. It is believed that the trivalent Cr-oxide is highly concentrated on the outer passive film for the HN stainless steel.

We previously reported that relatively thin Cr rich films were formed up to pH 3.3, above which the thicker Fe rich films were mainly found on the type 310S stainless steel [21]. As seen in Fig. 4a and b, the presence of metallic Fe and Cr to pH 4.3 indicates that the formed passive layer of the HN stainless steel is relatively thin even at the pH 4.3. Again, it is interesting that the trivalent Cr-oxide is a predominant element constituting the passive film up to pH 4.3 for the HN stainless steel.

At pH 5.5, on the contrary, the Fe-oxides were predominant, whereas the Fe metal was not seen in Fig. 4a. The relative intensities of the trivalent Cr-oxide and metal were also diminished in Fig. 4b; the calculated cationic ratio of Cr-oxide versus Fe-oxides was close to 0.2 in Fig. 5. The Fe-oxides were pretty enriched on the outer surface in Fig. 6d. The amount of Fe was concentrated to around 30% in atomic concentration after sputtering for 12 s. The amount of Cr was also concentrated to around 30% after sputtering for 60 s. The thickness of the passive layer was corresponded to around 7 nm from the depth profile (Fig. 6d).

Sagara et al. [24] reported that nitrogen was concentrated in the interface between passive film and HN stainless steel bulk after the polarization at 700 mV (SCE) in the artificial chloridic solution. Truman [25] found the nitrogen of steel is transformed to NO_3^- in the aqueous solution. Komori and Nakata [26] suggested that pH values of the electrolyte decreased after the polarization test due to the presence of NO_3^- in the solution.

Nitrogen in nitrogen-bearing stainless steel is soluble in aqueous solution [10]. The dissolution gives rise to the formation of NO_3^- at noble potential [14,25–28]. Yashiro et al. [28] clarified that the amount of NO_3^- increased after the polarization at elevated potential as high as 0.55 V (SCE). From the point of view, it is possible to think the following reaction on the cathode side, where the polarization tests were done at 600 mV (SCE)

$$N + 3H_2O \rightarrow NO_3^- + 6H^+ + 5e^- \quad (1)$$

The nitrogen in the stainless steel is oxidized to NO_3^- with simultaneous formation of H^+, and, it, in turn, would reduce the interfacial pH. As a result, Fe-oxides constituting the passive film at pH 4.3 would be dissolved in the presence of the NO_3^-. Therefore, the trivalent Cr-oxide could be mainly observed with the Cr metal component at pH 4.3 in Fig. 6b, implying the thickness of film is relatively thin.

We mentioned that ICR values vary with the structure of passive layer of stainless steel in Fig. 3. The as-polished HN stainless steel delivered lower ICR value. The passive layer was thin and Fe-oxides constitute the majority of the passive film. Thin passive layers based on Cr-oxide were obtained at pHs 2.3 and 4.3. Provided that the thickness of the films is similar among the three samples, the obtained ICR values should be close when the thickness factor is considered. Nonetheless, the measured ICR values were higher around 10 times for the cases of pHs 2.3 and 4.3. From this fact,

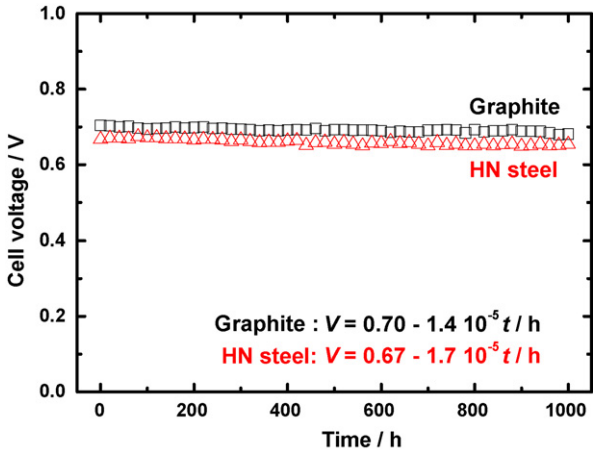

Fig. 7. Comparison of cell voltage for 1000 h operation at a current of 0.5 A cm^{-2} (348 K). Different bipolar plates, HN stainless steel and graphite, were employed for the operation.

it seems that the chemical composition of the passive film plays an important role to determine the resistance. For example, those films (pHs 2.3 and 4.3) are apparently thinner than the layer formed at pH 5.5. The thicker layer that is expected to have higher resistance obviously exhibited the similar ICR values comparing with those films formed at pHs 2.3 and 4.3 in Fig. 3, because the semiconducting Fe-oxides occupying a major portion of the passive layer reduce resistance. On the other hand, the higher portion of Cr-oxide provides significant corrosion resistance due to the existence of insulating Cr-oxide layer on the outer surface, which contributes to the maintenance of operation voltage. From the point of view, the HN stainless steel is expected to provide a good cell performance at a long term.

A single cell was fabricated using the HN stainless steel as bipolar plates and the cell was operated up to 1000 h at 348 K. For the operations, carbon cloth type GDL was used. The initial voltage was about 0.67 V at 0.5 A cm^{-2} (12.5 A) in Fig. 7. The observed voltage decay was about 17 mV after the operation for 1000 h. Graphite bipolar plates employing single cell exhibited the voltage decay of about 14 mV after 1000 h cell operation in Fig. 7. Even though the initial voltage was slightly lower comparing with the graphite bipolar plates employing single cell, the HN stainless steel adopting cell presented comparable performance to the graphite bipolar plates employing cell. As we previously reported [21], the type 304 and 310S bipolar plates employing cells showed voltage decays of 46 mV and 22 mV in 1000 h cell operation, respectively. Compared with our previous results, it is possible to think that the HN stainless steel would has better corrosion resistance than the type 304 and 310S stainless steels.

The HN stainless steel bipolar plates were carefully disassembled after 1000 h operation, and the ribs of gas inlet, center, and

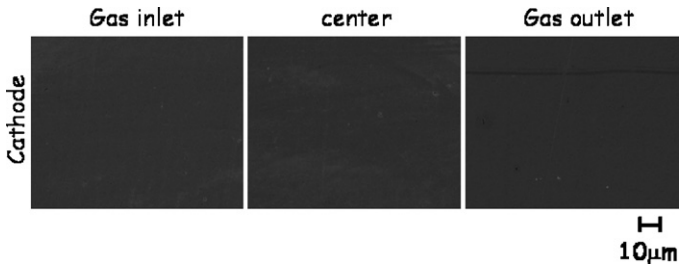

Fig. 8. SEM images of the rib surfaces of the HN stainless steel bipolar plates after 1000 h operation. The scale bar indicates 10 μm.

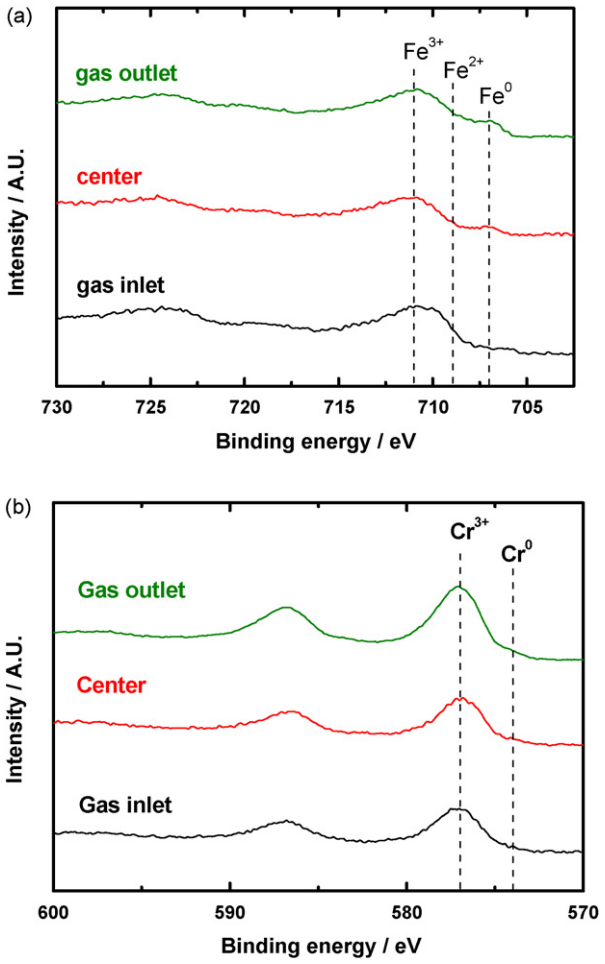

Fig. 9. XPS spectra of (a) Fe2p and (b) Cr2p for the HN stainless steel bipolar plate on cathodic side after 1000 h cell operation.

outlet parts selected from the bipolar plates were observed by SEM. Fig. 8 shows SEM images of rib surfaces of the bipolar plates for the cathode side after 1000 h cell operation. No trace of corrosion was observed in the cathode side after the cell operation for 1000 h. HN stainless steel possesses only 4 mass% of Ni in Table 1, while the Ni content for the type 310S stainless steel is around 20 mass% [21]. It is, therefore, thought that the good cell performance of the HN

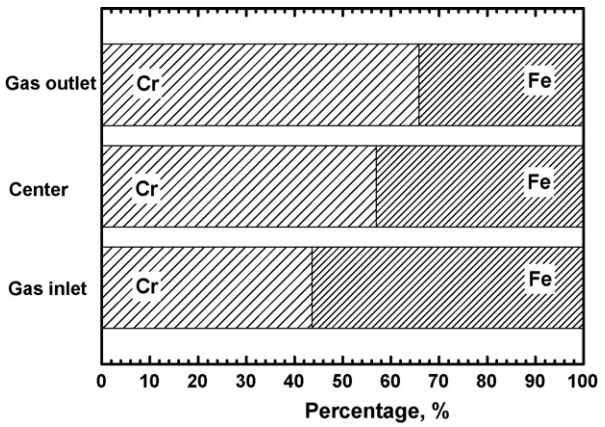

Fig. 10. Cr/Fe oxides cationic ratio in the outermost oxide layer of the HN stainless steel bipolar plate on cathodic side after 1000 h cell operation.

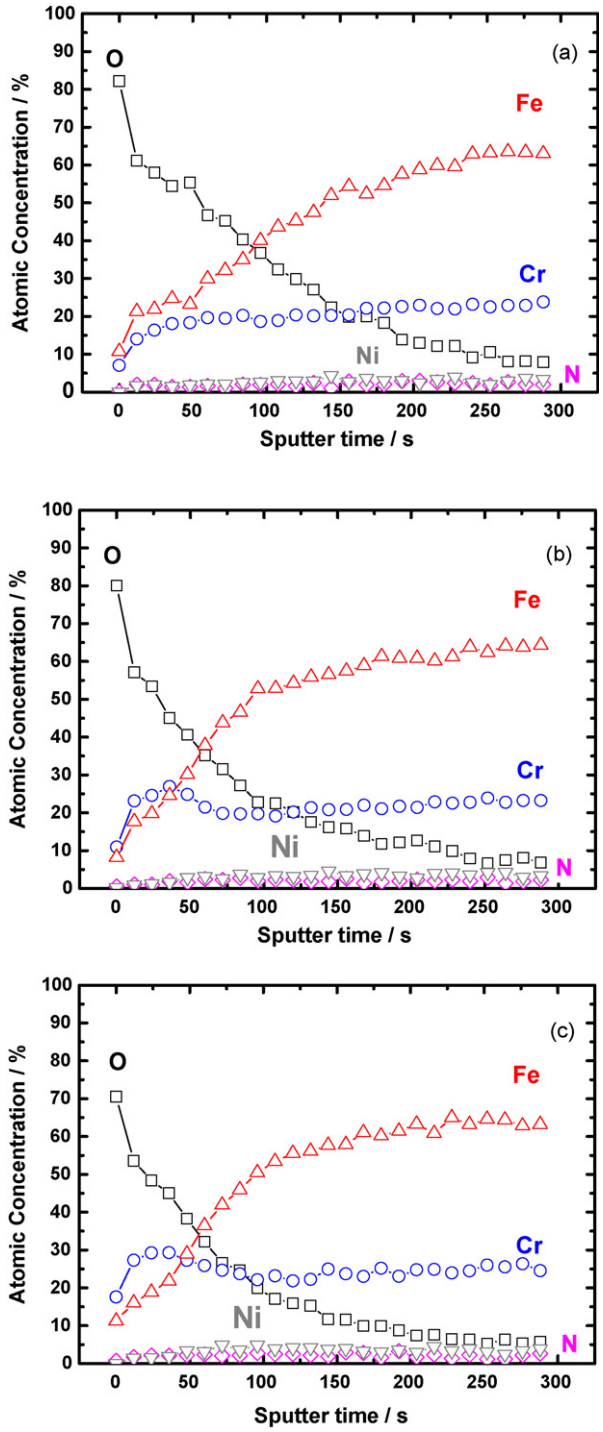

Fig. 11. XPS depth profiles of the HN stainless steel bipolar plate on cathodic side for (a) gas inlet, (b) center, and (c) gas outlet parts after 1000 h cell operation.

stainless steel employing cell could result in the excellent corrosion resistance achieved by the inclusion of nitrogen into the stainless steel.

Fig. 9 shows XPS spectra for the bipolar plate of cathode side after the cell operation for 1000 h. The observation was carried out on the three regions of the bipolar plate: the gas inlet, the center and the gas outlet parts. Although the Fe metal was not clearly observed around 707 eV, the Fe-oxides were observed around 711 eV as major component at the gas inlet in Fig. 9a. The Cr metal was also hardly seen at around 574 eV, but the trivalent Cr-oxide peak is observed around 577 eV for the gas inlet in Fig. 9b. Slightly large portion of Fe-oxides (cationic ratio of Cr-oxide versus Fe-oxides = 43:57) were detected in the most outer passive layer for the gas inlet (Fig. 10). From the depth profiles of the gas inlet part in Fig. 11, it is interpreted that the Fe and Cr ingredients are concentrated approximately to 17% and 25% in the outer surface, respectively, after sputtering for 36 s. The thickness of passive film was estimated to be 7–8 nm. The presence of relatively large amount of the Fe-oxides would be responsible for the thicker passive layer. The similar result was observed in the simulated condition at pH 5.5 (Fig. 6c). Combination of the simulated and the real environmental analyses suggested that the fuel cell environment during the 1000 h operation might have kept the pH higher than 4.3 in the gas inlet part.

Metallic Cr and Fe ingredients were present for the center and gas outlet parts in Fig. 9a and b. Intensities of the Fe-oxides spectra were slightly lower compared with that in the gas inlet part of Fig. 9a. Furthermore, the relative intensities of the trivalent Cr-oxide peak for the center and the gas outlet were somewhat higher than that of the gas inlet in Fig. 9b. The cationic ratio of Cr-oxide against Fe-oxides for the most outer surface was 57:43 for the rib in the center part and 66:34 in the gas outlet in Fig. 10, indicating that the trivalent Cr-oxide are prevalent on the outer surface for the gas outlet part. The atomic concentration of Cr in the center part was concentrated as high as 26% by sputtering for 36 s in Fig. 11b. The corresponding Fe content reached almost 24%. From the depth profile, the thickness of passive film ranged about 4–5 nm. For the gas outlet, the amount of Cr approached about 30% after sputtering for 36 s in Fig. 11c. The thickness of passive film was calculated to be around 4–5 nm. From the above results, the presumed pH values for the center and gas outlet parts may lay close 4.3 rather than 5.5. However, the pH value for the gas outlet part might be slightly lower than that for the center part since the Cr-oxide/Fe-oxides ratio was lower than that of center part in Fig. 10. From the XPS investigation, we found out that the passive film in the gas inlet part is composed of relatively thicker Fe-oxides. Almost equivalent amount of Cr- and Fe-oxides makes a harmony to form the outer surface for the center. For the gas outlet, the formed passive film is thin and is mainly constituted by trivalent Cr-oxide.

From the XPS analyses, it is proposed that the thin Cr-oxide layer is located on the outer passive layer and the Fe-oxides are placed under the thin Cr-oxide layer, after which metal bulk appears. Therefore, the semiconducting Fe-oxides layer would lead to the higher voltage, and the corrosion resistive Cr-oxide layer contributes to the retention of the higher voltage upon operation. The synergetic effect of the passive layer would be responsible for the excellent performance of the HN stainless steel as bipolar plates for PEFCs.

4. Conclusions

HN high nitrogen austenitic stainless steel was examined as bipolar plates for PEFCs. Even though the contained Ni was only around 4 mass% in the steel, the corrosion resistance measured in the synthetic solutions was comparable to the type 310S stainless steel, which contains about 20 mass% of Ni [20]. The improved corrosion resistance of the HN stainless steel, consequently, made it possible to maintain the higher voltage throughout the operation at 0.5 A cm^{-2} (12.5 A) for 1000 h, showing voltage decay of about 17 mV. No significant corrosion was seen in the HN stainless steel bipolar plates after the single cell operation for 1000 h. XPS analyses revealed that the passive film of rib surfaces for the center and gas outlet parts of the bipolar plates were enriched by the trivalent Cr-oxide. Relatively higher amount of Fe-oxides were observed for

the passive film of the gas inlet part. Summarizing the above results, it is concluded that the presence of thin Cr-oxide passive layer provides a good corrosion resistance and it is substantially effective to retain the higher cell voltage during the fuel cell operation.

Acknowledgement

The authors thank Ms. Miwa Watanabe, Iwate University, for her helpful assistance in the experimental works.

References

[1] F. Barbir, PEM Fuel Cells, Elsevier, 2005.
[2] R.L. Borup, N.E. Vanderborgh, Mater. Res. Soc. Symp. Proc. 393 (1995) 151.
[3] D.P. Davies, P.L. Adocock, M. Turpin, S.J. Rowen, J. Appl. Electrochem. 30 (2000) 101.
[4] L. Ma, S. Warthesen, D.A. Shores, J. New Mater. Electrochem. Syst. 3 (2000) 221.
[5] H. Wang, G. Teeter, J. Turner, J. Electrochem. Soc. 152 (2005) B99.
[6] A.K. Iversen, Corros. Sci. 48 (2006) 1336.
[7] Y. Wang, D.O. Northwood, Int. J. Hydrogen Energy 32 (2007) 895.
[8] K. Osozawa, N. Okato, in: R.W. Stahele, H. Okada (Eds.), Passivity and its Breakdown on Iron and Iron Base Alloys, NACE, 1976, p. 135.
[9] R.F.A. Jargelius-Pettersson, Corrosion 30 (1998) 162.
[10] M.A. Strecher, J. Electrochem. Soc. 103 (1956) 375.
[11] Y.C. Lu, R. Bandy, R.C. Newman, J. Electrochem. Soc. 130 (1983) (1774).
[12] S.J. Pawel, E.E. Stabsbury, C.D. Lundin, Corrosion 45 (1989) 125.
[13] H.P. Leckies, H.H. Uhlig, J. Electrochem. Soc. 113 (1966) 1262.
[14] C. Voigt, H. Werner, M. Gunzel, R. Simmchen, Corrosion 22 (1991) 3.
[15] G.C. Palit, V. Kain, H.S. Gadiyar, Corrosion 49 (1993) 977.
[16] K. Osozawa, Zairyo-to-Kankyo 47 (1998) 561.
[17] H. Wang, J. Turner, J. Power Sources 180 (2008) 791.
[18] Y. Katada, M. Sagara, Y. Kobayashi, T. Kodama, Mater. Manuf. Process. 19 (2004) 19.
[19] Japan Automobile Research Institute, NEDO Report (12-17-013-2-0002-2), 2001, p. 21.
[20] C.D. Wagner, W.M. Riggs, L.E. Davis, J.F. Moulder, Handbook of X-ray Photoelectron Spectroscopy, PerkinElmer Corp., Physics and Electronics Division, Eden Prairie, MN, 1979.
[21] M. Kumagai, S.-T. Myung, S. Kuwata, R. Asaishi, H. Yashiro, Electrochim. Acta 53 (2008) 4205.
[22] H. Tawfik, Y. Hung, D. Mahajan, J. Power Sources 163 (2007) 755.
[23] C.-O.A. Olsson, D. Landolt, Electrochim. Acta 48 (2003) 1093.
[24] M. Sagara, Y. Katada, T. Kodama, T. Tsuru, Nihon-Kinzoku-Gakkaishi 67 (2003) 67.
[25] J.E. Truman, Proc. UK Corrosion (1987) 111.
[26] T. Komori, M. Nakata, 4th International Congress on High Nitrogen Steels, ISIJ 32, 1995.
[27] H. Baba, T. Kodama, Y. Katada, Corros. Sci. 44 (2002) 2393.
[28] H. Yashiro, D. Hirayasu, N. Kumagai, ISIJ Int. 42 (2002) 1477.